We are IntechOpen, the world's leading publisher of Open Access books Built by scientists, for scientists

4,800
Open access books available

122,000
International authors and editors

135M
Downloads

Our authors are among the

154
Countries delivered to

TOP 1%
most cited scientists

12.2%
Contributors from top 500 universities

CLARIVATE ANALYTICS BOOK CITATION INDEX INDEXED

WEB OF SCIENCE™

Selection of our books indexed in the Book Citation Index in Web of Science™ Core Collection (BKCI)

Interested in publishing with us?
Contact book.department@intechopen.com

Numbers displayed above are based on latest data collected.
For more information visit www.intechopen.com

12

Error analysis and simulator in cylindrical near-field antenna measurement systems

Burgos Sara, Sierra-Castañer Manuel, Martín Fernando,
Cano Francisco and Besada José Luis
Technical University of Madrid (Universidad Politécnica de Madrid - UPM)
Spain

1. Abstract

Large antennas need special measurement systems because of their considerable dimensions. Typically, cylindrical near-field systems are appropriate measurement systems for omnidirectional antennas due to the characteristics of their radiation patterns. Furthermore, these systems are also appropriate for sizeable RADAR antennas, since they can be measured on their azimuthal positioner and the probe can be easily translated through a vertical linear slide. Thus, mechanical aspects of measurement systems are rather important since errors in the mechanical set-up can directly affect far-field radiation patterns.

This chapter presents an error estimation tool to analyze the most important errors for large L-band RADAR antennas in an outdoor cylindrical acquisition system and the effect of these errors in the calculated far-field radiation pattern. This analysis can be very convenient to evaluate the error budget of the Antenna Under Test (AUT).

The simulator computes the far-field with an array of vertical dipoles over a ground plane and compares an ideal infinite far-field with the electric field obtained using the cylindrical near-to-far-field (NF-FF) transformation algorithm. The influence of the inaccuracies on the final results is evaluated by introducing random and systematic sources of errors and then, analyzing the variations produced in the principal far-field patterns, antenna parameters and in the side lobe levels (SLL). Finally, this simulator can be employed to analyze the errors for L-band RADAR antennas.

One of the objectives of this investigation is thus to analyse how mechanical and electrical inaccuracies could affect the results of a cylindrical antenna measurement system, in order to minimize them as much as possible. This is highly important not only to meet the specifications, but also to reach high accurate results. There are several error sources studies for near-field patterns: the most complete are the ones developed by Joy and Newell in [Joy, 1988], [Newell, 1988], [Newell & Stubenrauch, 1988] and Hansen in [Hansen, 1988]. Later on, other investigations have been carried out analyzing precise error studies.

Another goal is the a-priori uncertainty analysis of these errors in the measurement of L-band RADAR antennas, detecting which are the main error sources for each antenna

parameter and calculating the uncertainty budget. Finally, ground reflections were analyzed by means of simulations.
These errors appear due to the grating lobes of the RADAR antennas when the peak value of the radiation pattern is orientated towards extreme angular positions (out of system specifications). Through simulations, it is possible to evaluate the effect of the grating lobes: distortion, ripple, influence of the reflections in the side lobes closer to the zenith or in the main lobe… To finish, a method based on a diagnostic technique for cancelling the effect of the reflections is presented. This work has been applied to an existing outdoor antenna measurement facility. This facility was designed by the authors and it is being used for the characterization of L-band RADAR antennas.

2. Introduction

Large antennas need special measurement system due to their considerable dimensions. This study presents the error analysis for large L-band RADAR antennas performed for a cylindrical outdoor measurement system. In the literature, there are some works previously published about cylindrical near-field systems – i.e. [Romeu et al., 1990], [Romeu et al., 1992], [Broquetas et al., 1994] −, although most of them deal only with the near-to-far-field transformation algorithm. This transformation can be based on different approaches.
In 1978, Borgiotti presented in [Borgiotti, 1978] an integral formulation using a superposition of plane waves to obtain the far-field from the measured near-field. Later, in the works published by Hansen in [Hansen J.A., 1980], by Yaghjian in [Yaghjian, 1986] and in [Rudge et al., 1982], a second methodology was detailed. In this case, the scattering matrix formulation is employed to derive the coupling equation. A third approach, introduced by Brown and Jull in [Brown & Jull, 1961] and Leach and Paris in [Leach & Paris, 1973], is based on the three-dimensional vector cylindrical wave expansion of an electromagnetic field which applies the Lorentz reciprocity theorem formulation to attain the complete vector far-field pattern of an arbitrary antenna. In addition to the procedure proposed by Leach, Bucci in [Bucci, 1988] and Hussein and Rahmat-Samii in [Hussein & Rahmat-Samii, 1993] studied some improvements in efficiency of this method. In the last years, some approaches to solve the problem of near-to-far-field transformation using equivalent currents have been presented, i.e. [Petre & Sarkar, 1992], [Sarkar & Taaghol, 1999], [Blanch et al., 1995], [Las Heras et al., 2002], [Las Heras et al., 2005].
The first objective of this investigation is to analyse how the mechanical and electrical inaccuracies could affect the results of a cylindrical antenna measurement system, in order to minimize them as much as possible. This is highly important not only to fulfil the specifications, but also to reach a high accuracy in the results. There are several studies of the error sources for near-field patterns: the most complete are the ones developed by Joy in [Joy, 1988], Newell in [Newell, 1988] and in [Newell & Stubenrauch, 1988] and by Hansen in [Hansen J.E, 1988].
Later on, other investigations have been carried out analyzing particular error studies. The one presented in the First AMTA Europe Symposium – [Pivnenko et al., 2006] − could be an example.
The second objective is the analysis of these errors in the measurement of L-band RADAR antennas, detecting which are the main source of errors for each parameter. This study has been applied to the facility described in [Martín, 2006] and in [Burgos, 2006]. The maximum length of the array antenna (up to 12 meters) requires a particularly large antenna measurement system.

As mentioned before, since cylindrical near-field ranges are appropriate to measure large antennas, the system considered is a cylindrical near-field range. In such facility, the RADAR antennas rotate on its own positioner and the probe (double-polarized probe) moves along a 15.5 meters linear slide, stopping on each defined position to acquire the near-field. In addition, the AUT can work in reception and transmission and can operate with a sum or a difference monopulse pattern.
The last aim of this research is to evaluate the effect of ground reflections on the final results. This is particularly important for this kind of antennas and antenna measurement system: when peak values of the radiation patterns of the RADAR antenna are oriented towards extreme angular positions, grating lobes of the RADAR antennas can appear and produce errors due to reflections in the facility ground. To analyze the grating lobes influence, simulations were carried out. Finally, a method based on a diagnostic technique for eliminating the effect of the reflections is applied, the reflections are located and the radiation pattern is improved.
This chapter is divided in the following parts. First, *section 2* details the introduction. Then, *section 3* summarizes three different points. The first one explains the near-to-far-field transformation algorithm and its validation. Next, the error simulator for a cylindrical near-field system and the evaluation of the results are presented. The last point of *section 3* describes an error analysis of the L-Band RADAR antenna measurement system. After that, *section 4* analyses the effect of the grating lobes and studies an algorithm for cancelling the effect of reflections. Finally, in *section 5* the conclusions and future researches are drawn.

3. Error Simulator for a Cylindrical Near-Field System and Evaluation of the Results

In order to evaluate the performances of this error simulator, first the near-to-far-field transformation algorithm is studied and validated. Then, some of the results achieved from the simulations are presented. Finally, a detailed error analysis of a real L-Band RADAR antenna measurement system based on Montecarlo simulations is commented.

3.1 Near-to-Far-Field Transformation Algorithm and its Validation

In [Burgos, 2008], the description of the cylindrical near-to-far-field transformation, considering probe correction, its validation and its application is explained. By using Reciprocity Theorem, the electric field can be expressed as a combination of the four weighting functions (for AUT and probe), obtaining the expression proposed by Leach and Paris in [Leach & Paris, 1973]:

$$\begin{aligned} v(\rho_o,\varphi_o,z_o) &= \frac{\kappa^2}{4\pi^2 k^2}\sum_{n=\infty}^{\infty} e^{\,jn\varphi_o}\cdots \\ &\int_{\infty}^{\infty}\left(a_n(h)\sum_{m=\infty}^{\infty} c_m(-h)H_{n+m}^{(2)}(k\rho_o)+b_n(h)\sum_{m=\infty}^{\infty} d_m(-h)H_{n+m}^{(2)}(k\rho)\right)\cdots \\ &e^{\,jhz_o}dh \end{aligned} \tag{1}$$

where:
- "n" indicates the modal index (integer number),

- "*h*" symbolizes the propagation constant in the z-direction (real number) h=k·cosθ,
- "*k*" characterizes the wave number in free space,
- $\kappa=\sqrt{(k^2-h^2)}=k\cdot\sin\theta$ is the projection of the propagation constant in the *xy*-plane,
- $H^{(2)}_{n+m}(k\rho_0)$ denotes the cylindrical Hankel function of 2nd kind and order n+m,
- $a_n(h)$ and $b_n(h)$ correspond to the AUT weighting functions of the TE- and TM-modes,
- $c_m(h)$ and $d_m(h)$ represent the probe modal coefficients.

The model developed for this application introduces the probe compensation method proposed by Hansen in [Hansen J.A., 1980], and usually applied to the spherical near-to-far-field transformation algorithms. Assuming the rotationally symmetry of the antenna probe (μ=±1), the probe pattern is calculated from the main planes of the probe diagram. For this particular case, the antenna probe is a conical corrugated horn that fulfils the previous condition. The first step is the calculation of the co-polar far-field of the antenna probe in the principal planes $E_e(\theta)$ and $E_h(\theta)$. The θ- and ϕ-components of the electric field at each angular position are obtained through:

$$\begin{aligned}
E_{1,\theta}(\theta,\phi) &= E_e(\theta)\cos\phi + P_1\cdot E_e(\theta)\sin\phi \\
E_{1,\phi}(\theta,\phi) &= -P_1\cdot E_h(\theta)\cos\phi + E_h(\theta)\sin\phi \\
E_{2,\theta}(\theta,\phi) &= \frac{1}{A_{xy}}\left[P_2\cdot E_e(\theta)\cos\phi + E_e(\theta)\sin\phi\right] \\
E_{2,\phi}(\theta,\phi) &= \frac{1}{A_{xy}}\left[-E_h(\theta)\cos\phi + P_2\cdot E_h(\theta)\sin\phi\right]
\end{aligned} \tag{2}$$

where E_1 and E_2 represent the probe patterns for acquiring both polarizations. P_1 and P_2 symbolize the linear polarization ratio of the antenna probes, and A_{xy} the amplitude and phase factors of the signals coming from both probes. If single probe is used, P_1=-P_2 and A_{xy}=1. If an ideally polarized antenna is employed, P_1=P_2=0. If the coordinate systems of the measurement of the antenna probe are different to the coordinate systems of the cylindrical acquisition (i.e. a classical spherical far-field system is used), several angular rotations of the probe radiation pattern are required – using the method proposed in [Rahmat-Samii, 1979] – in order to obtain the probe compensated far-field radiated pattern. In addition, this method employs the Discrete Fourier Transform (DFT) instead of the Fast Fourier Transform (FFT). With this change, the far-field in the final coordinate system could be achieved without needing an interpolation of the radiation pattern results, although the processing time is a bit larger. *Fig. 1* summarizes the transformation algorithm applied for this application.

The previous tool has been validated using both simulations and measurements. The implemented procedure starts with the modelling of the transmitting and receiving antenna. The simulated AUT is an array of 28x16 λ/2 dipoles vertically displaced, over a ground plane at a distance equal to λ/4, and assumed to be infinite, so Image Theory can be applied. The excitation is separable in vertical and horizontal planes, and with decreasing amplitude to reduce the side lobe levels. Besides, in the horizontal plane, a phase error is added, in order to simulate a more realistic AUT. The total size of the simulated AUT is 5.3 m x 2.1 m. On the other hand, the antenna probe is a vertically polarized conical corrugated horn, and its main planes radiated fields obtained through the integration of the electric field on the aperture are:

$$\vec{E}_{ap} = \hat{y} J_0\left(\frac{2.405 r'}{a}\right) e^{-j\pi r'^2/\lambda L} \tag{3}$$

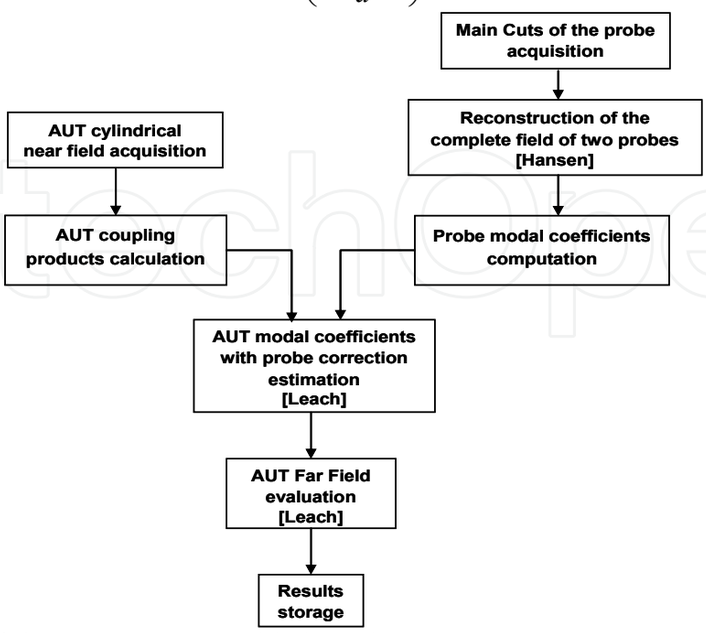

Fig. 1. Diagram of the Near-To-Far-Field algorithm

The acquisition is simulated on a cylinder where the distance from the AUT to the probe tower is 5 meters, the vertical path of the probe is 15 meters. The number of samples in the azimuth is 256 (to satisfy the Nyquist sampling theorem), while the distance between samples at the vertical axis is 10 cm. The frequency selected for the simulations 1215 MHz. The field in each point of the grid was calculated taking into account the field radiated by all the dipoles modified by the probe pattern. The field from each dipole in each point of the grid is given by the sum of 3 spherical waves, in the way explained in [Elliot, 1981]:

$$E_z = -j30 I_{mn}\left(\frac{e^{-jkR_1}}{R_1} + \frac{e^{-jkR_2}}{R_2} - 2\cos(kL_1)\frac{e^{-jkr}}{r}\right) \tag{4}$$

The induced voltage at the antenna probe can be calculated applying the expression (5), since each element of the array could be considered in far-field respect the antenna probe:

$$v \approx k.I_{mn}\left(\frac{e^{-jkR_1}}{R_1} f_s(\theta_1) + \frac{e^{-jkR_2}}{R_2} f_s(\theta_2) - 2\cos(kL_1)\frac{e^{-jkr}}{r} f_s(\theta)\right) \tag{5}$$

where k is a complex constant, I_{mn} is the dipole excitation, the angles and distances are shown in Fig. 2, and $f_s(\theta)$ is the radiation pattern of the probe. The far-field radiation patterns achieved for the main planes are compared with the infinite far-field, obtained by multiplying the array factor by the element radiation pattern, as Fig. 3 and Fig. 4 show. Fig. 3 and Fig. 4 show a significant concordance between both calculated patterns, so the NF-FF transformation could be considered validated. The small discrepancies in the extremes of

the horizontal angular range are due to the approximation of the acquisition model, shown in expression (4). This simulation tool is also useful for testing the elevation validity range of the NF-FF transformation, which is often approximated by the method proposed by Yaghjian [Yaghjian, 1975] and Newell [Newell & Crawford, 1974]:

$$\theta_0 = \tan^{-1}\frac{L_z - D}{2x_o} \tag{6}$$

where L_z indicates the path performed by the probe, D corresponds to the height of the AUT and x_0 is the separation between the probe and the AUT, as shown in Fig. 5.

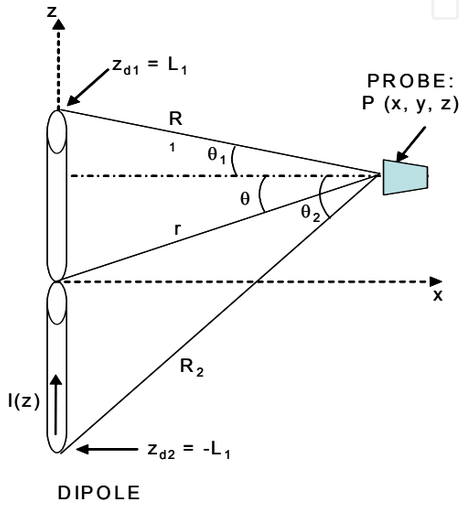

Fig. 2. Geometry of the dipole and probe

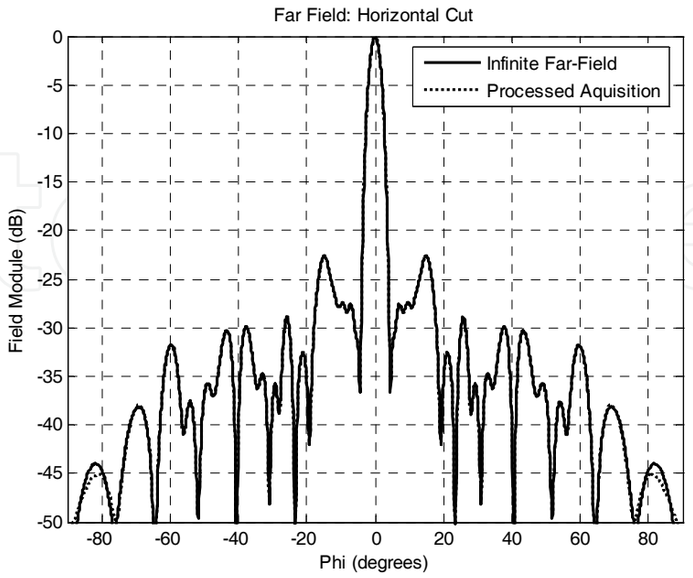

Fig. 3. Horizontal cut: Theoretical Far-field versus ideal NF-FF transformed pattern.

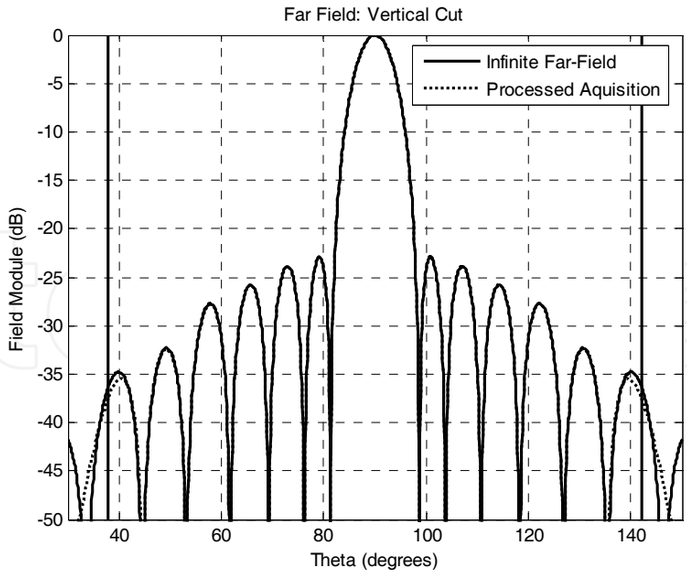

Fig. 4. Vertical cut: Theoretical Far-field versus ideal NF-FF transformed pattern.

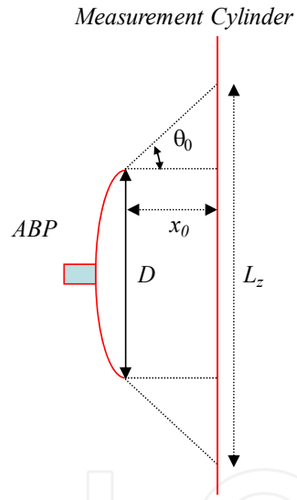

Fig. 5. Angular validity margin

With this configuration of the cylindrical system and the modelling of this specific AUT, the angular range of validity goes from 37.7 to 142.3 degrees. Fig. 4 confirms that the angular margin of the measurement is valid.

A measurement in the cylindrical near-field system of the Technical University of Madrid was performed to validate this algorithm. The AUT utilized was the Ku-band reflector shown in Fig. 6. This antenna was measured in both the spherical near-field system (using TICRA SNIFTD Software) and the cylindrical near-field system. The results from the comparison of the horizontal and the vertical cuts are illustrated in Fig. 7 and Fig. 8.

Fig. 6. Ku-band reflector employed for the validation measurements

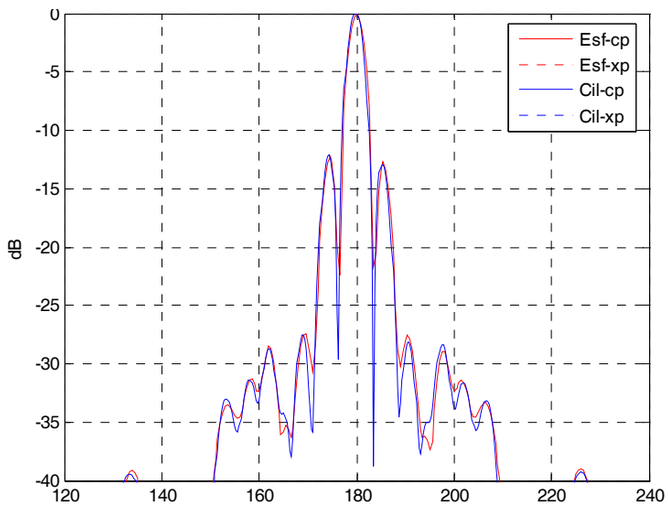

Fig. 7. Horizontal cut for the measurement with the Ku-reflector

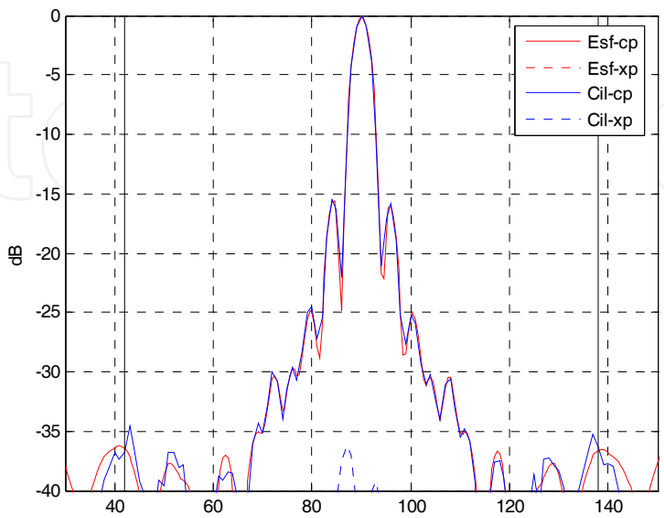

Fig. 8. Vertical cut for the measurement with the Ku-reflector

3.2 Error simulations

To evaluate how errors could affect the final results, a model of the antennas and a simulation of the acquisition process including errors has been performed. The simulator compares the outcomes achieved from the reference data (i.e. far-field obtained from an acquisition free from additional errors) with the ones including the deviations, as Fig. 9.

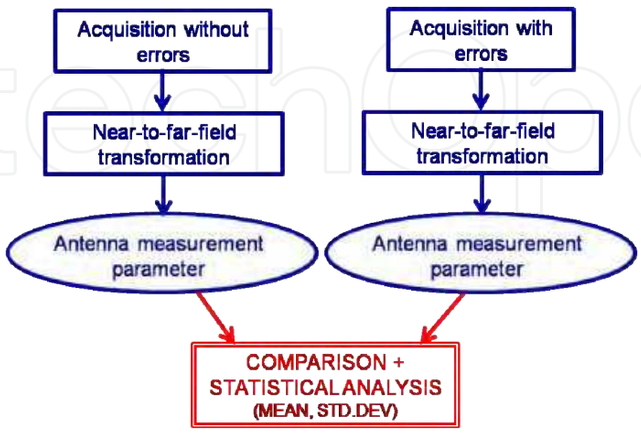

Fig. 9. Simulator diagram

For the uniform random error in probe x-, y- and z-position, an exhaustive study was completed and 10 iterations for each peak to peak amplitude were achieved for a RADAR L-Band antenna of 5.32 metres by 2.08 metres. From these simulations, it could be calculated the mean of the difference in peak directivity, which gives an estimation of the error, and the standard deviation of the difference in peak directivity, which gives an estimation of the uncertainty, as shown in Fig. 10 and Fig. 11. From these results, it can be observed that in both cases the deviations in the x-position of the probe have clearly larger influence on the mean and on the standard deviation of the differences in peak directivity. This is due to the fact that the AUT and the probe are aligned along the x-axis and thus the deviations in this direction produce larger errors.

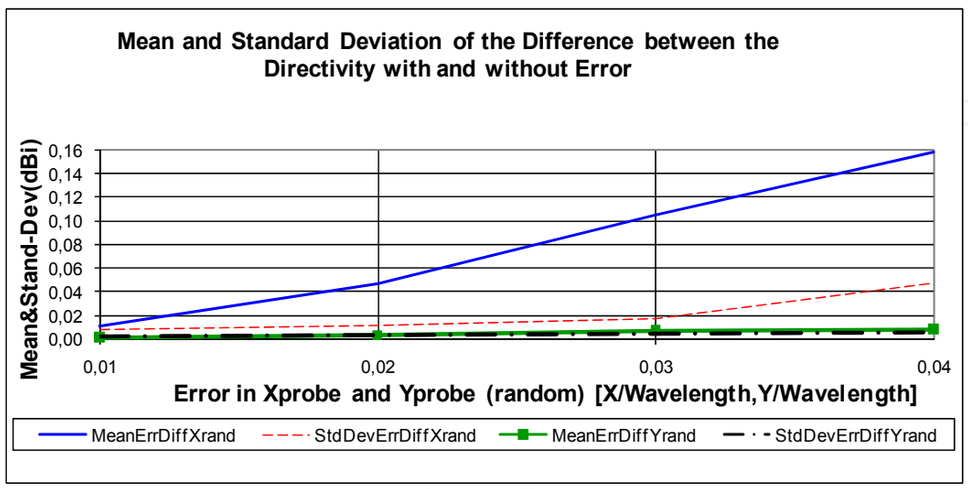

Fig. 10. Mean and standard deviation of the difference between the peak directivity with and without error, for errors in the x- and y-position of the probe

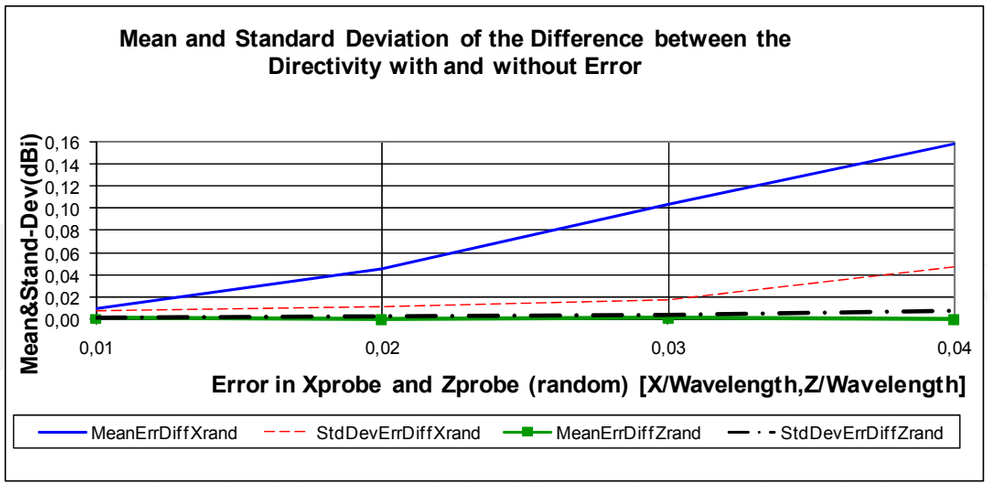

Fig. 11. Mean and standard deviation of the difference between the peak directivity with and without error, for errors in the x- and z-position of the probe

In order to verify that the errors in the *x*-position of the probe and the phase errors are comparable, the equivalent phase errors for the deviations in the *x*-position of the probe was calculated, as shown in Table 1. Fig. 12 and Fig. 13 represents the mean and the standard deviations of the directivity differences according to all the considered phases (the ones calculated from the deviations in the *x*-position of the probe and the ones taken into account in the phase deviations simulations).

Error in x-probe	0.01λ		0.02λ		0.03λ	0.04λ
Corresponding Phase	3.6		7.2		10.8	14.4
Phase Error	2	4	6	8		

Table 1. Evaluated phase errors and comparison with longitudinal errors along x-axis

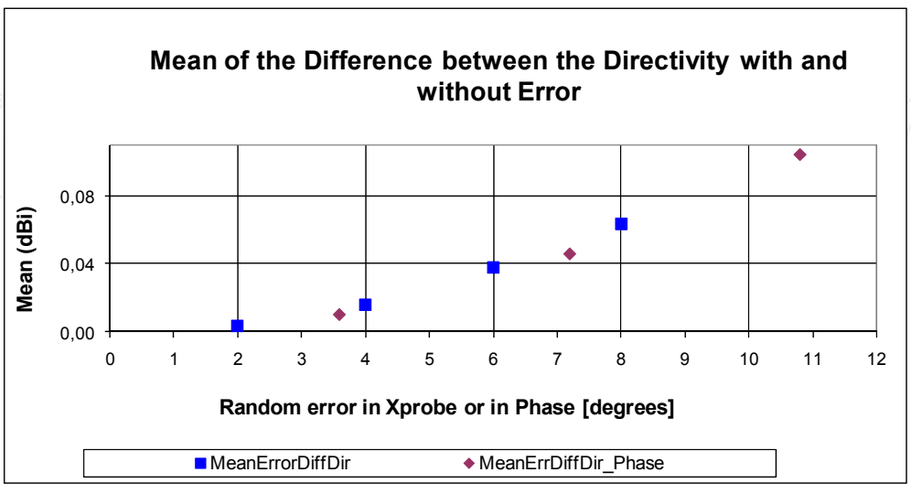

Fig. 12. Mean of the difference between the peak directivity with and without an error in the x-position of the probe and with a random phase error

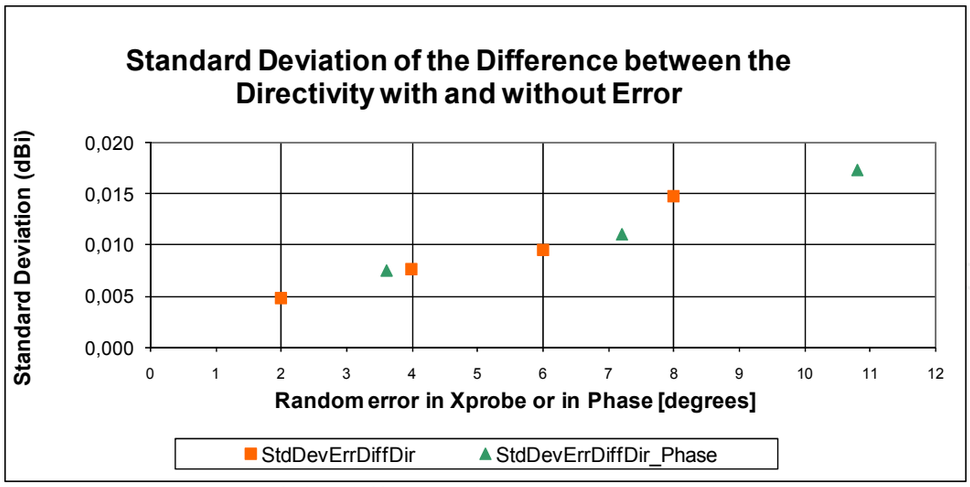

Fig. 13. Standard deviation of the difference between the peak directivity without and with an error in the x-position of the probe and with a random phase error

Since the mean and the standard deviation linearly vary as the errors increase, it can be deduced that the errors in the *x*-position of the probe and in the phase are comparable. As the second ones are easier to compute, the uncertainties due to mechanical deviations can be calculated in a faster way using the equivalent phase errors.
In order to analyze the influence of the antenna size in the statistical parameters (i.e. mean and standard deviation), achieved from the difference between the antenna parameter with and without error, simulations with five different antennas – shown in Table 2 – have been carried out.

	L (m)	H (m)	Excitation
Ant 1	1,52	0,52	Uniform
Ant 2	1,90	0,78	Uniform
Ant 3	2,66	1,04	Uniform
Ant 4	5,32	2,08	Uniform
Ant 5	7,22	2,86	Uniform

Table 2. Sizes of the antennas considered for the simulations

In this study, 10 iterations per case have been completed. This number is not enough to get error probability distributions, although it is good enough to analyze the trends. Fig. 14. and Fig. 15. correspond to representative results of the standard deviations of the difference between the directivity with and without error, when considering a random error in the *x*-position of the probe, and a random phase error or a white Gaussian noise for 5 antennas with uniform excitation, after 10 iterations. From the obtained results, it can be concluded that the uncertainty is lower as the antenna size is larger.

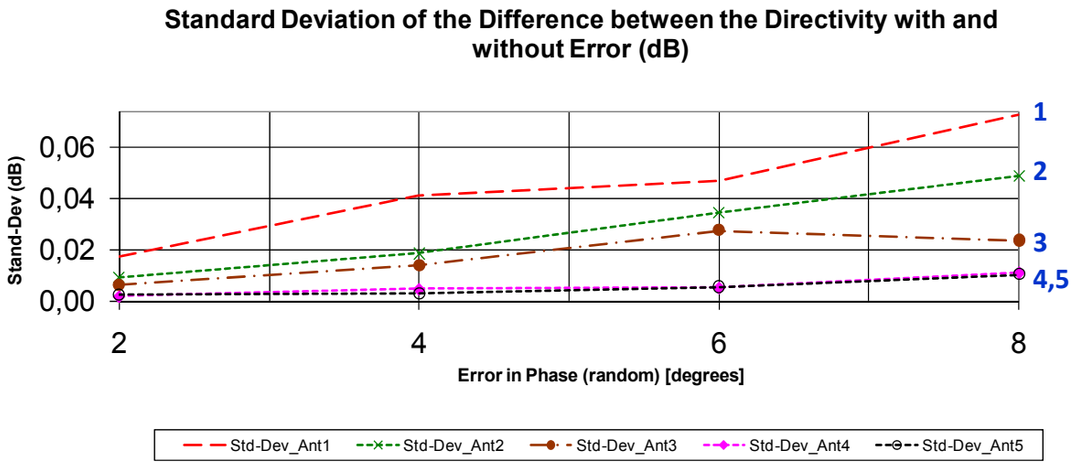

Fig. 14. Standard deviation of the difference between the differences in directivity without and with a random phase error

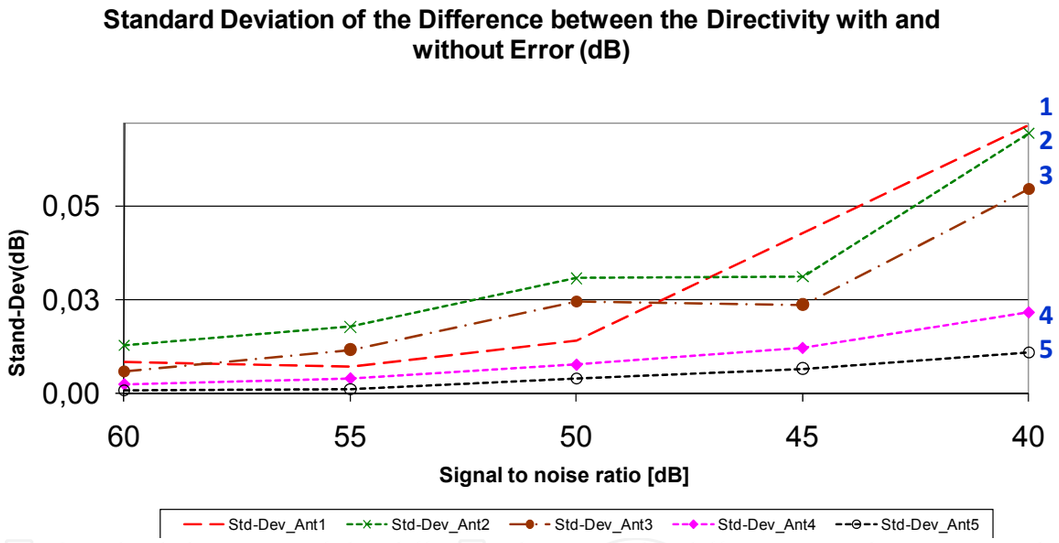

Fig. 15. Standard deviation of the difference between the differences in directivity without and with a white Gaussian noise (WGN)

Fig. 16 and Fig. 17 represent some examples of the statistical analysis in the SLL when considering a random phase error or a WGN for 5 antennas with different sizes and with uniform excitation after 10 iterations.

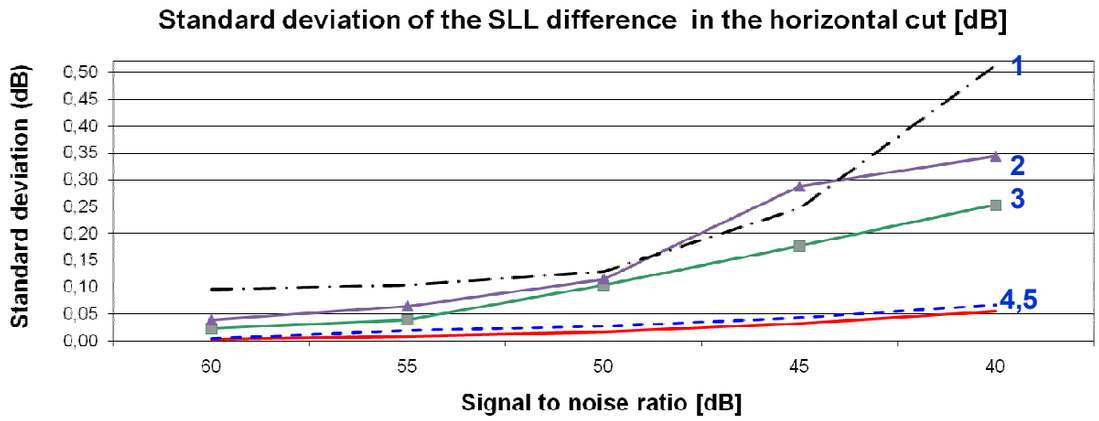

Fig. 16. Standard deviation of the difference between the differences in SLL without and with WGN

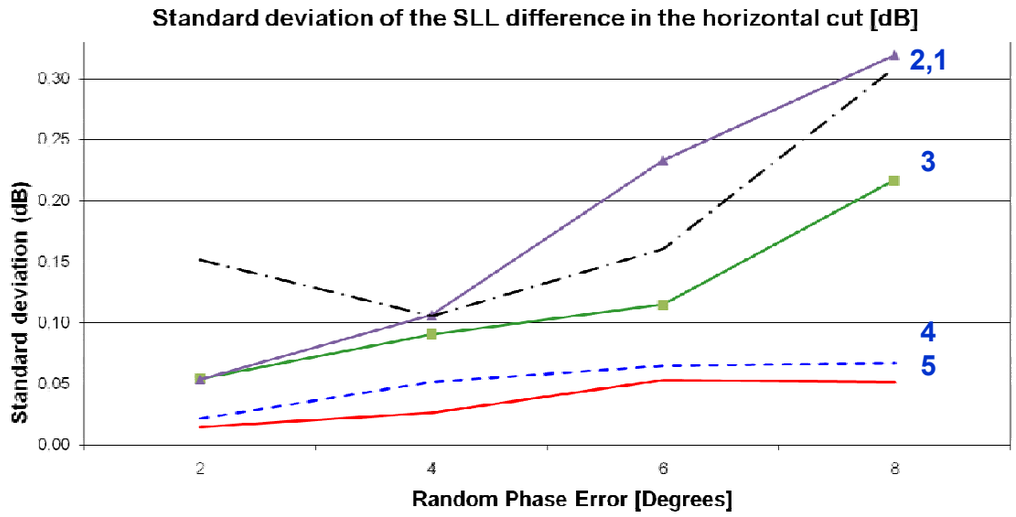

Fig. 17. Standard deviation of the difference between the differences in SLL without and with a random phase error

From the results obtained, it can be observed that the means and the standard deviations are larger for the smallest antennas (antenna 1 and antenna 2) and smaller for the biggest antennas (antennas 4 and 5).

3.3 Error Analysis of the L-Band RADAR Antenna Measurement System: Montecarlo Simulations

Typical calculations of uncertainties and systematic errors in antenna measurements are based on the calculation or estimation of the standard deviation and mean of each error term respectively. In this particular case, a Montecarlo study with one hundred iterations per antenna excitation was implemented, including some error sources. The study calculates the inaccuracies in the next main antennas parameters: directivity, pointing directions, SLL and beamwidth. In order to carry out a more detailed analysis, two different antennas were simulated. The antennas are not centered in the measurement range.

Their main dimensions (length and height) and some of the parameters of the measurement range (position of the tower respect to the antenna, length of the tower and valid angular range of the measurement results) of these two scenarios are detailed in Table 3:

RADAR	Long. [m]	Height [m]	x_o [m]	L_z [m]	Mech. Tilt [deg]	$\theta_{v,min}$ [deg]	$\theta_{v.max}$ [deg]
Antenna 1	5.32	2.08	5.0	15.5	16.1	20.9	123.2
Antenna 2	11.78	6.82	7.0	15.5	10	42.1	110.1

Table 3. Antenna dimensions and parameters of the measurement system

Besides, it is worth noting that for this case, different amplitude distribution – sum and difference patterns, electric tilt… – were examined:

- Sum amplitude distribution in the horizontal and in the vertical planes,
- Sum amplitude distribution in the horizontal plane and difference amplitude distribution in the vertical plane,
- Difference amplitude distribution in the horizontal plane and sum amplitude distribution in the vertical plane.

These cases were studied with the antenna 1 mechanically tilted 16.1 degrees and with electrical tilt of 0 or 40 degrees in the vertical plane. In the case of antenna 2, this is mechanically tilted 10 degrees, and there is not any electrical tilt.

As commented before, the results obtained with the simulator show the comparison between the ideal far-field radiation pattern (no errors were added) with the far-field radiation pattern including errors. In this analysis, the probe correction was omitted to reduce the computational time of the simulations. Besides, the AUT was mechanically tilted from the vertical axis, as it happens in the measurement. The simulator allows representing the histograms of the different parameters. For instance, Fig. 18 to Fig. 20 show the histograms of the sum pattern distribution for antenna 1.

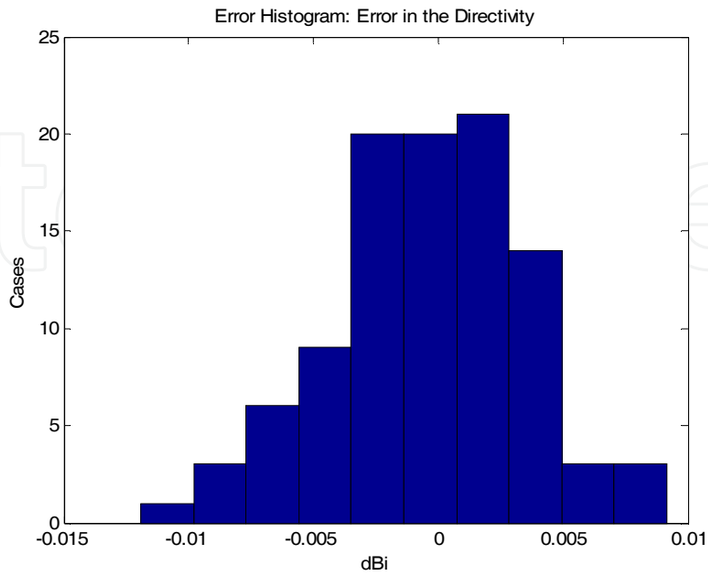

Fig. 18. Histogram of the error in the directivity

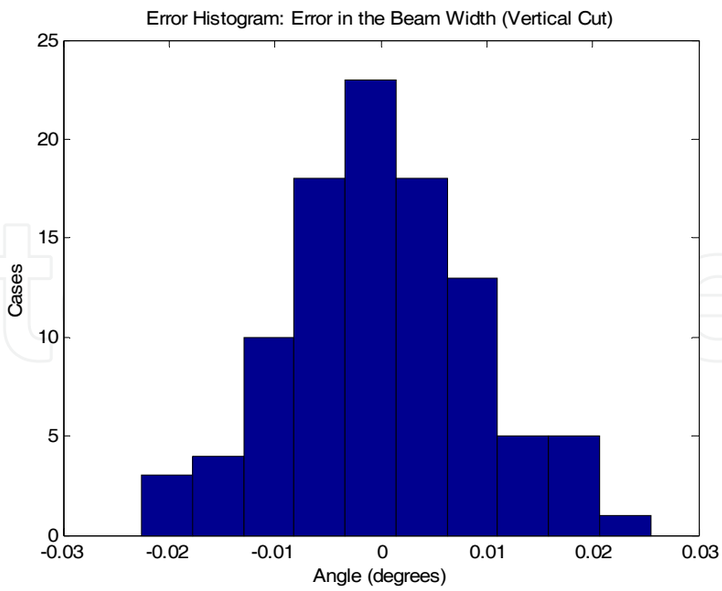

Fig. 19. Histogram of the error in the beam width in the vertical cut

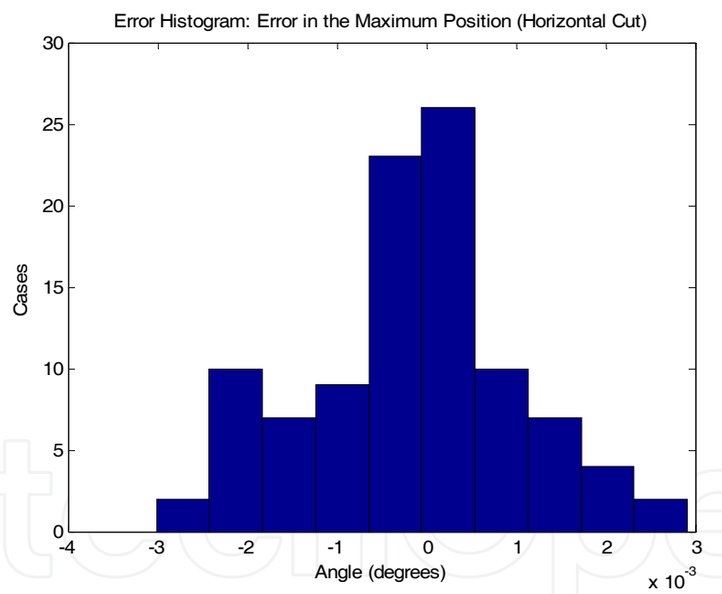

Fig. 20. Histogram of the error in the position of the maximum in the horizontal cut

In addition, the Montecarlo study was completed with the analysis of the statistics achieved from the 100 iterations. The next table summarizes the results obtained for Antenna 1 and Antenna 2 when no electrical tilt is designed:

PARAMETER	QUANTITY	RMS ERROR	MAXIMUM ERROR
Directivity (dBi)	39.86	0.0036	0.2762
Beam Width in the Horizontal Cut (degrees)	1.51	$3.85\ 10^{-5}$	0.0016
Beam Width in the Vertical Cut (degrees)	2.46	$6.30\ 10^{-5}$	0.0026
SLL (-20 dB to -30 dB)	–	–	1.1 dB
SLL (-30 dB to -40 dB)	–	–	2.0 dB
Position of the maximum in the Horizontal Cut (degrees)	0	$3.65\ 10^{-5}$	$7.85\ 10^{-4}$
Position of the maximum in the Vertical Cut (degrees) for the sum pattern	80.0	$5.52\ 10^{-5}$	0.0014
Position of the null in the Vertical Cut (degrees) for the difference pattern	80.0	$1.00\ 10^{-5}$	$3.47\ 10^{-4}$

Table 4. Results obtained in the Montecarlo study for the antenna 2

In conclusion, when the antenna is bigger, the errors found with the Montecarlo simulations were smaller for all the parameters, except for the directivity and side lobe level, where they were larger.

4. Reflections study

Since the cylindrical near-field system under study is an outdoor range, an important error factor is the reflections on the environment, particularly the effect of the ground. In this section, an analysis of the effect of the reflections in the ground plane and a method to reduce this effect are presented. Measurements on an L-Band RADAR antenna are shown.

4.1 Effect of Grating Lobes

During a measurement campaign some negative effects due to the ground reflection were detected. These errors appear as a ripple in the far-field obtained. These errors are due to the grating lobes of the RADAR antennas when the peak value of the radiation pattern is orientated towards extreme angular positions and they are operating at highest frequencies (out of the operation frequency range).

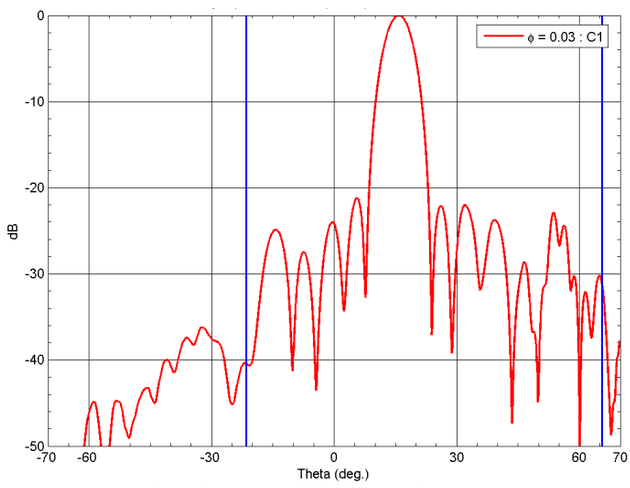

Fig. 21. Measurement without reflections in the ground

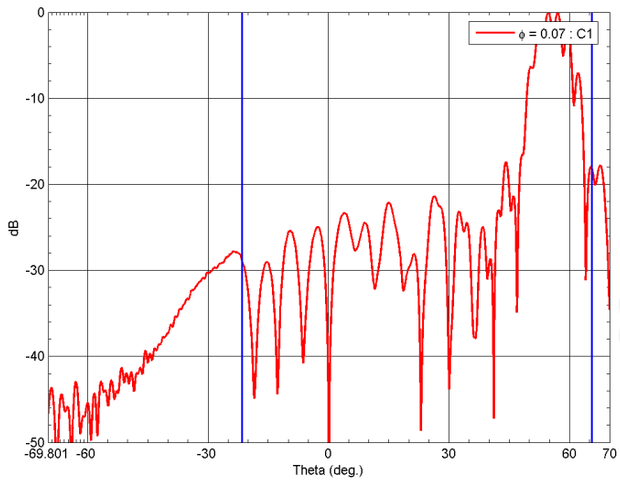

Fig. 22. Measurement with reflection in the ground (Higher tilt and higher frequency)

Several simulations have been carried out to confirm that the reflections are the cause of ripple problem. The first one consisted in increasing the antenna beam pointing at elevation, from 0 to 40 degrees at the centre of the frequency band, using different reflection coefficients (from 0 to -1). Results depicted in Fig. 23 show the higher the pointing is, the more affected the acquired near-field appears. This perturbation creates a ripple in the far-field, even noticeable in the main lobe, when the electrical tilt is 40 degrees. In fact, at 40 degrees the near-field is so affected that the main lobe of the far-field is completely degraded.

For the electrical tilt of 40 degrees, the frequency was varied. Fig. 24 concludes that the higher the frequency is, the more important the ripple is. Therefore, the grating lobes and their reflections on the ground plane are the responsible of the far-field ripple observed in the measurements. According with equation (7), these grating lobes appear at higher tilt and frequency for this antenna structure.

$$\theta = a\cos\left(\frac{N2\pi - \alpha}{kd}\right) \tag{7}$$

- k is the wave number,
- d represents the distance between array elements in vertical,
- α corresponds to the progressive phase,
- N symbolizes an integer number.

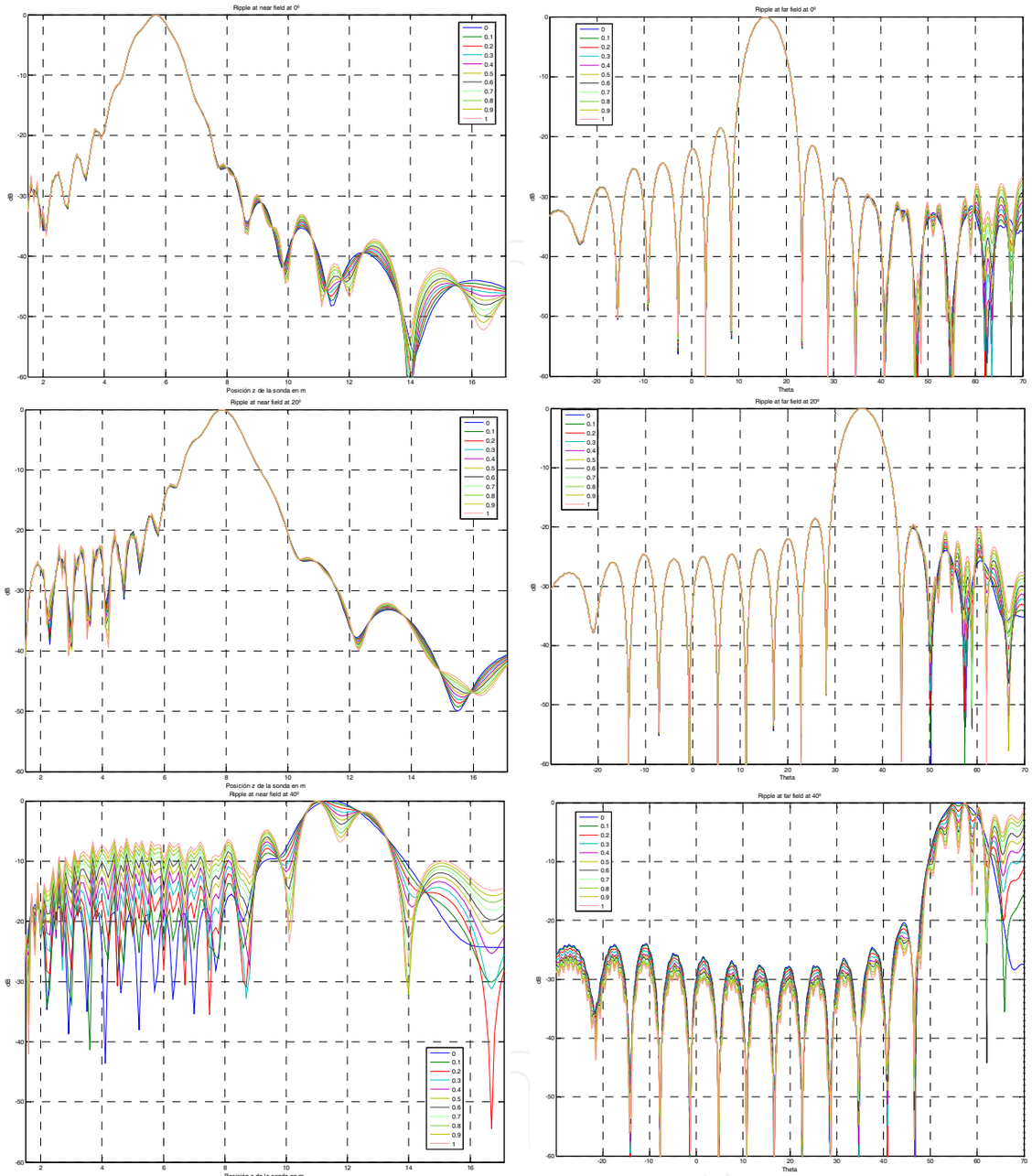

Fig. 23. Simulations of vertical plane near-field acquisitions and their transformed far-field at the centre of the frequency band and varying electrical pointing from 0 to 40 degrees (mechanical tilt 16 degrees)

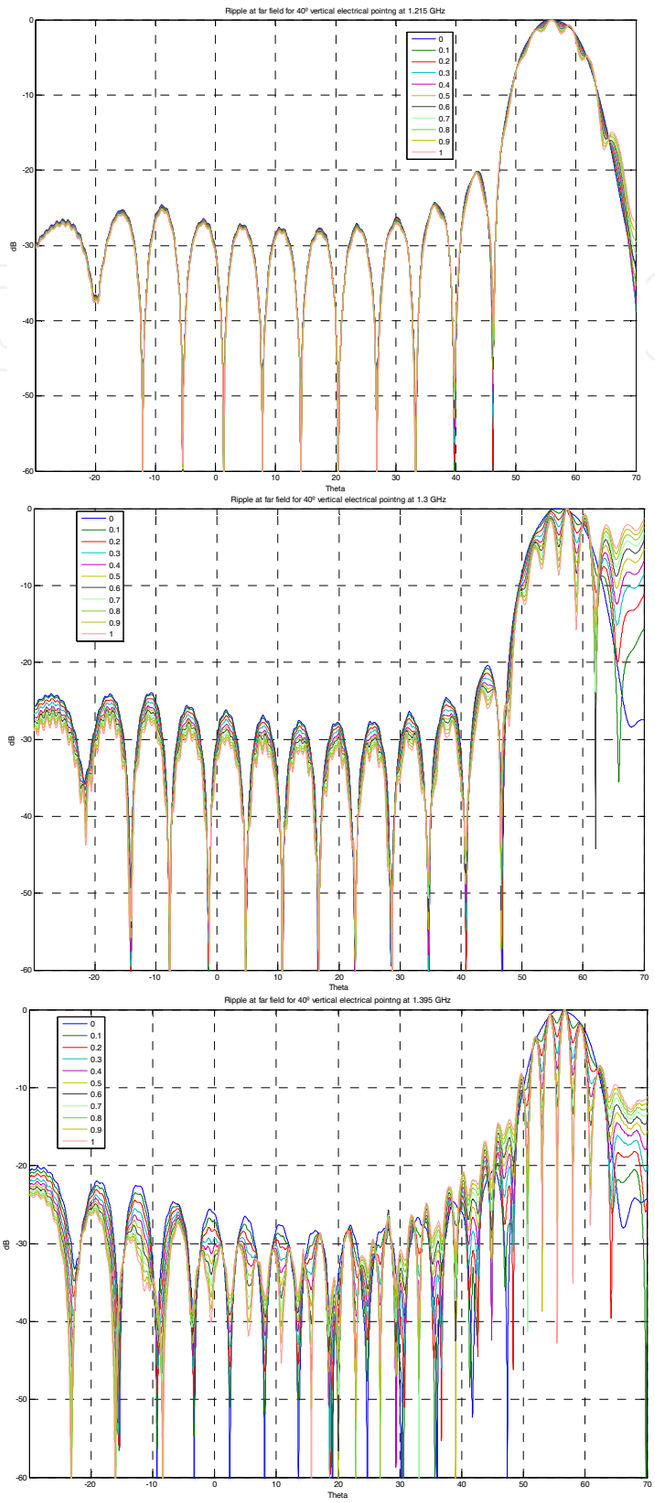

Fig. 24. Simulations of vertical plane far-field at 40 degrees of vertical pointing varying the frequency (1215, 1300 and 1395 MHz) along the band (mechanical tilt 16 degrees)

4.2 Diagnostic techniques for Cancelling the Effect of Reflections

As it has been seen in the previous section, the effect of reflections disturbs the results of the radiation pattern, especially when the frequency and the tilt angle are high. There are several ways to reduce such effect, but the most popular and always used in anechoic chamber, is the use of radiation absorbent material (RAM). Since the measurement range is an outdoor cylindrical near-field system, it is not the most suitable solution, and it is necessary to use a measurement processing technique to reduce the effect of the reflections. Different kinds of these processing techniques have been proposed and tested, being two of them the most effective. The first one is based on the "Matrix-Pencil Method", used to approximate signals into a sum of complex exponentials. Then, the exponential functions are processed to identify the terms corresponding to the different propagating components. Once identified, the terms corresponding to the reflected components are removed. The theory of this technique was presented in [Sarkar & Pereira, 1995] and applied to the reflection cancelling problem in [Fourestié et al., 1999]. The second technique is called "FFT-Based Method" and estimates the impulse response of the measured environment from its frequency response by using the inverse Fourier transform. In the time domain, the direct contribution is detected, eliminating the undesired echoes. This method was studied by [Loredo et al., 2003] and compared with the first one in [Loredo et al., 2004]. The main problem of both techniques is the necessity to measure in a frequency band that produces an important increase of the measured time.

To reduce the acquisition time, an algorithm which only needs the information in a frequency is applied. Such algorithm is based on a diagnostic technique which is a method to obtain the extremely near-field or the equivalent currents distribution of an antenna from the knowledge of its radiated field (near or far-field). With this information, it is possible to detect errors, and also to identify which are the causes of such errors, for example, electrical errors in arrays or mechanical errors in reflectors. The presence of these errors is always detected in the far-field pattern, when it is seen that a difference between the real case and the design case exists. However, to identify errors in the AUT could be a very hard and long task for the antenna designer. So, in this case it is interesting to use one of these techniques to reduce the difficulty and the time in the design stage. This is the typical and classical application of a diagnostic process. However, it is also possible to use a diagnostic technique in other applications, like reflection cancelling, as shown in [Cano et al., 2009]. The steps of the proposed method to reduce the effect of the reflections are indicated below.

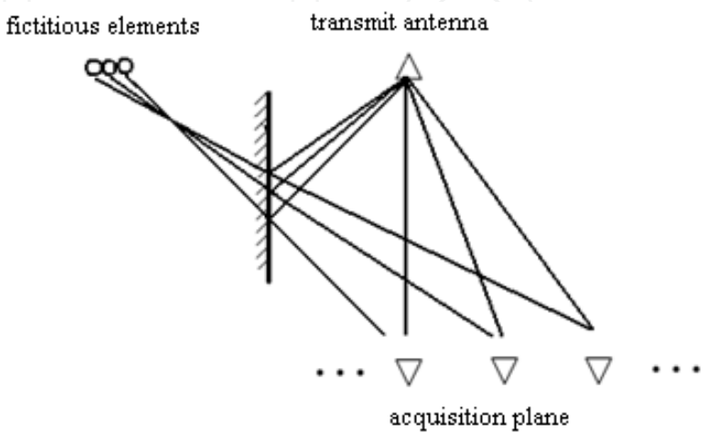

Fig. 25. Fictitious elements which appear when there are reflections.

- First of all, a diagnostic process is applied and the extremely near-field in a zone larger than the antenna dimensions is obtained. Out of the antenna, a "fictitious field" appears due to the reflection on the environment, as it can be seen in Fig. 26.
- After that, the field value out of the antenna dimension is set to zero, removing the effect of the reflections.
- Finally, from the filtered field, a new plane wave spectrum is recalculated where the ripple due to the reflections has disappeared. With this information the θ and ϕ components of the far-field is obtained by means of the expressions (8) and (9).

$$E_\theta = j\lambda \frac{e^{-jkr}}{r}\left(P_x \cos\phi + P_y sen\phi\right) \tag{8}$$

$$E_\theta = j\lambda \frac{e^{-jkr}}{r}\left(P_x sen\phi - P_y \cos\phi\right) \tag{9}$$

where "P_x" and "P_y" are the components of the plane wave spectrum, "λ" is the wavelength and "k" is the wavenumber.

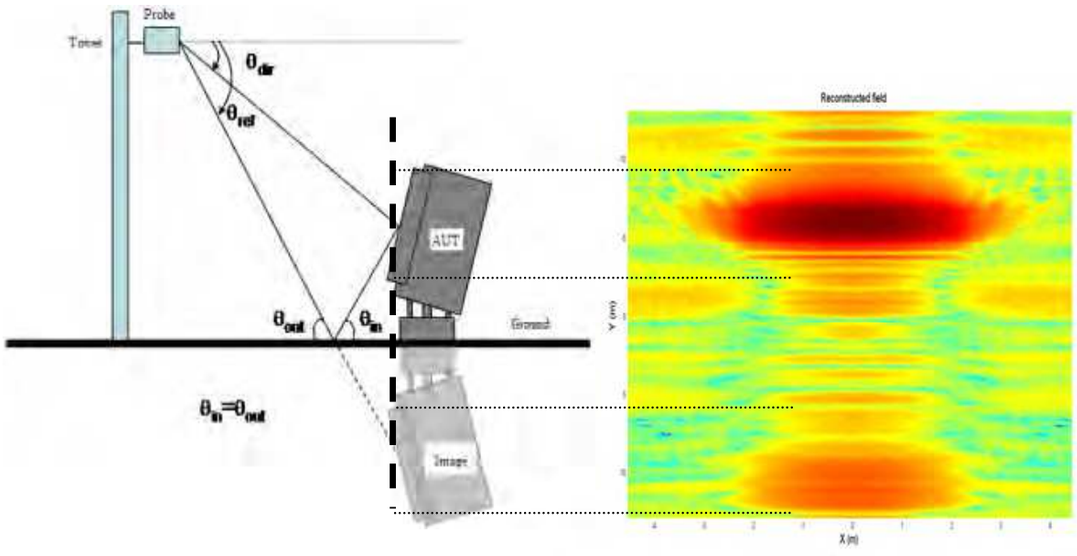

Fig. 26. Reconstructed field over the antenna plane (f = 1.22 GHz, tilt = 30º).

Once the reflection cancelling technique has been explained, the following stage is to apply it to the RADAR measurements and to verify that the effect of reflections is less important. As it has been indicated in the previous section, the reflection level depends on the frequency and the tilt angle, so the proposed technique will be applied to two different cases, varying both mentioned parameters. Firstly, the measurement with a frequency equal to 1.22 GHz and a tilt angle equal to 30 degrees is taken, and after applying the technique, the results depicted in the following figures are obtained.

The Fig. 27 represents the reconstructed field over the antenna plane, where it is possible to observe the presence of reflections. The next figure, Fig. 28, shows the effect of the reflections in the radiation pattern and also the result after applying the reflection cancelling technique, where it can be seen that the ripple due to reflections disappears.

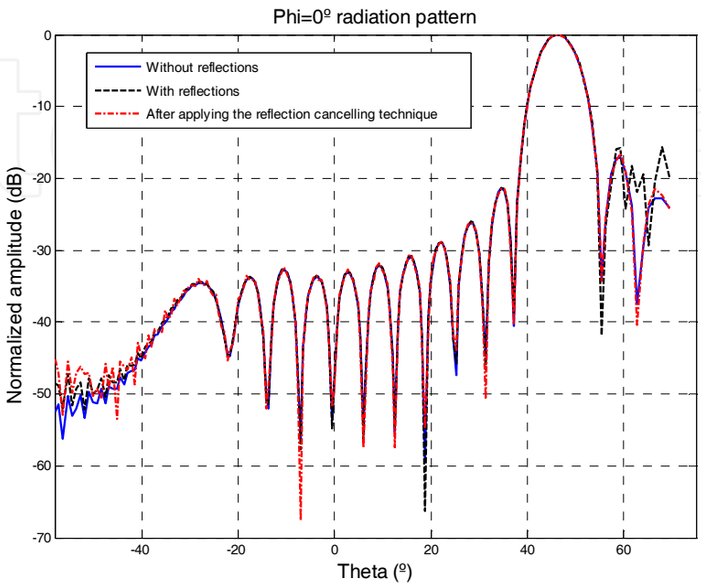

Fig. 27. Radiation pattern comparison with and without reflections and applying the reflection cancelling technique (f = 1.22 GHz, tilt = 30º).

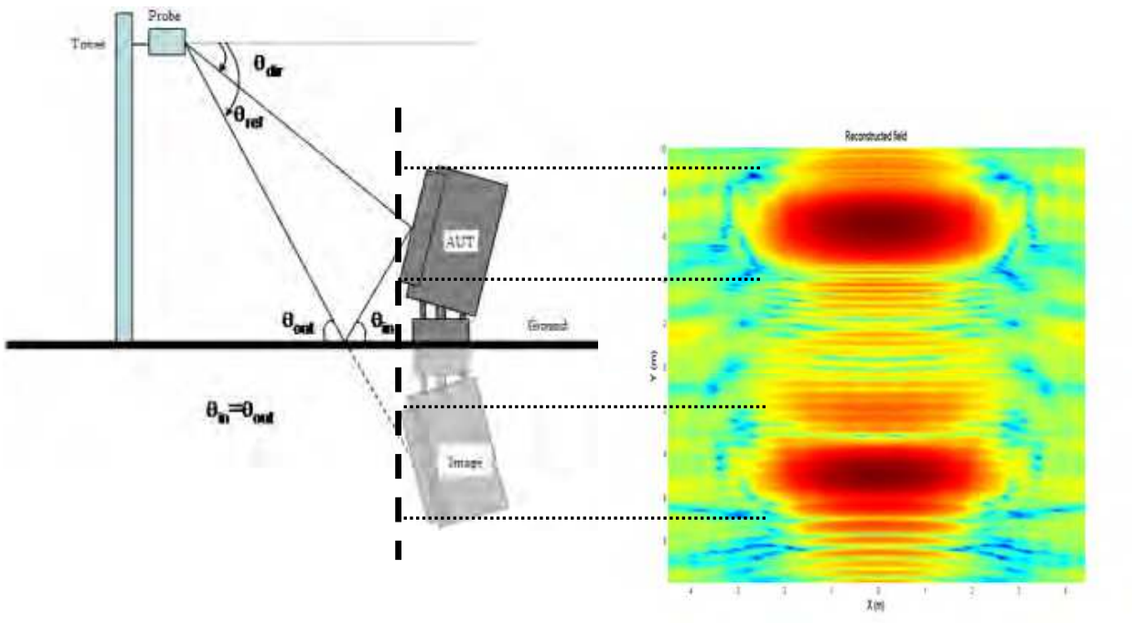

Fig. 28. Reconstructed field over the antenna plane (f = 1.4 GHz, tilt = 40º).

Next, the same results are presented for the case of a frequency equal to 1.4 GHz and a tilt angle equal to 40 degrees. As it can see in Fig.29, the fictitious field amplitude is higher because the measurement has been performed with a higher frequency and a larger tilt, so the grating lobe is directly steered to the ground plane.

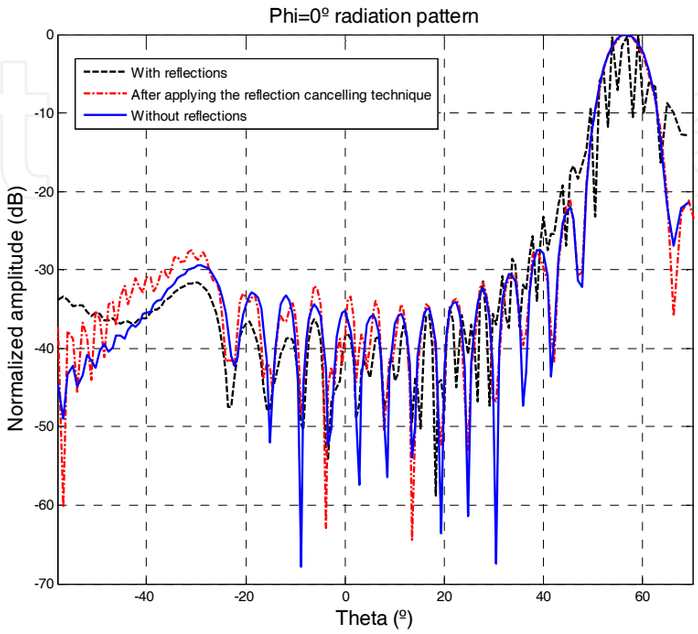

Fig. 29. Radiation pattern comparison with and without reflections and applying the reflection cancelling technique (f = 1.4 GHz, tilt = 40º).

5. Conclusions and Future Researches

The implemented simulator for this investigation allows characterizing uncertainties in the antenna parameters according to the kind of antenna and the mechanical and electrical system performances. With the error simulation in acquisition achieved using this tool, the analysis of their effects on some of the main antenna parameters (i.e. far-field radiation pattern, directivity, SLL) has been carried out.

While considering random errors, if several iterations are carried out, a statistical analysis allows obtaining the mean and the standard deviation of the errors that respectively gives an estimation of the error and the uncertainty produced. Since the AUT and the probe are aligned along the x-axis of the probe, the random errors in the x-direction are the ones that have a larger influence in the antenna parameters. This effect can be simulated as an error phase equivalent to $\Delta\phi \cong -k_o \Delta x$.

The uncertainty in the peak directivity decreases if the antenna size increases when considering a random deviation in the x-probe position a random phase or a WGN. In addition, the mean and the uncertainty of the error in SLL in both vertical and horizontal cuts are larger for the smallest antennas and less significant for the largest antennas when including a random change in the x-position of the probe, a random phase or a WGN.

Furthermore, Monte-Carlo simulations with one hundred iterations were performed to check the effect of the sum of different error sources in the antenna parameters. The results showed that whereas the errors in the directivity or SLL were larger with a bigger antenna, almost all the errors in the other type of parameters were smaller with this antenna.

Apart from mechanical and electrical deviations, in this work the effect of ground reflections has been analyzed. These errors appear due to the grating lobes of the RADAR antennas when the peak value of the radiation pattern is orientated towards extreme angular positions and in the upper extreme of the frequency band. It was observed that the grating lobes and their reflections on the ground plane were the responsible of ripples in the far-field radiation patterns.

In order to cancel the effect of the ground reflections, a method based on a diagnostic technique has been applied. Such algorithm allows obtaining the extremely near-field or the equivalent currents distribution of an antenna from the knowledge of its radiated field. With such information, it is possible to detect errors, and also to identify the causes of these deviations. As seen from the results, the implemented technique reduces the ripple due to the reflections.

Some interesting future researches could be evaluate other sources of errors, such as for example AUT support scattering, the amplitude non-linearity or the truncation errors. In addition, other cancelling techniques could be analyze with the intention of minimizing errors, such as mechanical errors, electrical errors, acquisition errors, processing errors or stray signals.

6. References

Blanch, S.; Jofre, L.; Romeu, J. (1995). Comparation Between Classical and Equivalent Current Apprach Near-Field to Far-Field Transformation, Antenna and Propagation Society International Symposium, AP-S. Digest, Vol.1, Iss., 18-23, Jun. 1995, pp. 260-263.

Borgiotti, G. V. (1978). Integral Equation Formulation for Probe Corrected Far-Field Reconstruction from Measurements on a Cylinder, IEEE Transactions on Antennas and Propagation, Vol. AP-26, No. 4, July 1978, pp. 572-578.

Broquetas, A.; Romeu, J.; Rius, J. M.; Elias-Fuste, A. R.; Cardama, A.; Jofre, L. (1994). An approximate expression to estimate signal-to-noise improvement in cylindrical near field measurements, IEEE Transactions on Antennas and Propagations, Vol 42, Nº7, June 1994, pp. 1007-1010.

Brown, J. & Jull, E. V. (1961). The Prediction of Aerial Radiation Patterns From Near-Field Measurements, Inst. Elec. Eng., Paper No. 3649 E, Nov. 1961.

Bucci, O. M. (1988). Use of Sampling Expansions in Near-Field-Far-Field Transformations: The Cylindrical Case, IEEE Transactions on Antennas and Propagation, Vol. 36, No. 6, June 1988, pp. 830-835.

Burgos, S.; Martín, F.; Sierra-Castañer, M.; Besada, J. L. (2006). Error Estimations In Cylindrical Near Field System For Large RADAR Antennas, European Conference on Antennas and Propagation (EuCAP) symposium proceedings, November 2006, Nice, France.

Burgos, S.; Martín, F.; Sierra-Castañer, M.; Besada, J. L. (2008). Cylindrical near-to-far-field transformation system for RADAR antennas: Design, validation and application, *Microwave and Optical Technology Letters*, Vol. 50, No. 10, October 2008, pp. 2527 – 2531.

Cano, F.; Sierra-Castañer, M.; Besada, J.L. (2009). Application of diagnostic technique for reflection cancelling in antenna measurement, European Conference on Antennas and Propagation (EuCAP) symposium proceedings, March 2009, Berlin, Germany.

Elliot, R. S. (1981). *Antenna Theory and Design*, Ed. Prentice-Hall, Inc., Englewood Cliffs, New Jersey.

Fourestié, B.; Altman, Z.; Wiart, J.; Azoulay, A. (1999). On the Use of the Matrix-Pencil Method to Correlate Measurements at Different Test Sites, IEEE Transaction on Atennas and Propagation, Vol. 47, No. 10, October 1999.

Joy, E. B. (1988). Near-Field Range Qualification Methodology, *IEEE Transactions on Antennas and Propagation*, Vol. 36, No. 6, June 1988, pp. 836-844.

Hansen, J. E. (1988). *Spherical Near-Field Antenna Measurements*, Peter Peregrinus Ltd. on behalf of IEE, ISBN: 0 86341 110 X, London, UK.

Hansen, J. A. (1980). On Cylindrical Near-Field Scanning Techniques, IEEE Transactions on Antennas and Propagation, Vol. AP-28, No. 2, March 1980, pp. 231-234.

Hussein, Z. A. & Rahmat-Samii, Y. (1993). Probe Compensation Characterization in Cylindrical Near-Field Scanning, IEEE, 1993, pp. 1808-1811.

Las Heras, F.; Galocha, B.; Besada, J. L. (2002). Far-Field Performance of Linear Antennas Determined From Near-Field Data, IEEE Transactions on Antennas and Propagation, Vol. 50, No. 3, March 2002, pp. 408-410.

Las Heras, F.; Galocha, B.; Besada, J. L. (2005). Circular Scanning and Equivalent Magnetic Currents for Main Plane Near-Field Transformation, International Journal of Numerical Modelling: Electronic Networks, Devices and Fields, Vol. 15, No. 4, July/August 2005, pp. 329-338.

Leach, W. M. Jr. & Paris, D. T. (1973). Probe Compensated Near Field Measurements on a Cylinder, IEEE Transactions on Antennas and Propagation, Vol. AP-21, No. 4, July 1973, pp. 435-445.

Loredo, S.; Rodríguez, M.; Las-Heras, F.; Sarkar, T.P. (2003). Cancelación de ecos en cámaras de medida no anecoicas, XXIV Simposium Nacional de la Unión Científica Internacional de Radio, URSI 2009.

Loredo, S.; Rodríguez, M.; Las-Heras, F.; Sarkar, T.P. (2004). Echo identification and Cancellation Techniques for Antenna Measurement in Non-Anechoic Test Sites, IEEE Antennas and Propagation Magazine, Vol. 46, No. 1, February 2004.

Martín, F.; Burgos, S.; Sierra-Castañer, M.; Besada, J. L. (2006). Design of a cylindrical near field system for RADAR antennas, European Conference on Antennas and Propagation (EuCAP) symposium proceedings, November 2006, Nice, France.

Newell, A. C. & Crawford, M. L. (1974). Planar near-field measurements on high performance array antennas, *Nat. Bur. Stand.*, NBSIR 74-380, July 1974.

Newell, A. C. (1988). Error Analysis Techniques for Planar Near-field Measurements, *IEEE Transactions on Antennas and Propagation*, Vol. 36, No. 6, June 1988, pp. 754-768.

Newell, A. C.; Stubenrauch, C. F. (1988). Effect of Random Errors in Planar Near-Field Measurements, *IEEE Transactions on Antennas and Propagation*, Vol. 36, No. 6, June 1988, pp. 769-773.

Petre, P. & Sarkar, T.K. (1992). Planar Near-Field to Far-Field Transformation Using an Equivalent Magnetic Current Approach, IEEE Transactions on Antennas and Propagation, Vol. 40, No. 11, Nov. 1992, pp. 1348-1356.

Pivnenko, S.; Nielsen, J. M.; Breinbjerg, O. (2006). Electrical Uncertainties In Spherical Near-Field Antenna Measurements, Proceedings of the First Antenna Measurements Techniques Association Europe (AMTA Europe) Symposium, pp.183-186, May 2006, Munich, Germany.

Rahmat-Samii, Y. (1979). Useful Coordinate Transformations for Antenna Applications, *IEEE Transactions on Antennas and Propagation*, Vol. AP-27, No. 4, July 1979, pp. 571-574.

Romeu, J.; Baquero, M.; Ferrando, M.; Jofre, L.; Alemany, J.; González, V. (1990). A Cylindrical near field test facility, Microwave Engineering Europe, September/October 1990, pp. 25-31.

Romeu, J.; Jofre, L.; Cardama, A. (1992). Far-field errors due to random noise in cylindrical near-field measurements, IEEE Transactions on Antennas and Propagations, Vol. 40, N^{o}1, June 1992, pp. 79-84.

Rudge, W.; Milne, K.; Olver, A.D.; Knight, P. (1982). The Handbook of Antenna Design, Vol 1, pp. 609-614, Peter Peregrinus Ltd. on behalf of IEE, ISBN: 0-906048-82-6, London, UK.

Säily, J.; Eskelinen, P.; Räisänen, A. V. (2003). Pilot Signal-Based Real-Time Measurement and Correction of Phase Errors Caused by Microwave Cable Flexing in Planar Near-Field Tests, *IEEE Transactions on Antennas and Propagation*, Vol. 51, No. 2, Feb. 2003.

Sarkar, T.K. & Pereira, O. (1995). Using the Matrix Pencil Method to Estimate the Parameters of a Sum of Complex Exponentials, IEEE Antennas and Propagation Magazine, Vol. 37, No. 1, February 1995.

Sarkar, T.K. & Taaghol, A. (1999). Near-field to Near/Far-field Transformation for Aribitrary Near-Field Geometry Utilizing an Equivalent Electric Current and MoM Antennas and Propagation, IEEE Transactions on Antennas and Propagation, Vol. 47, Iss. 3, Mar. 1999, pp. 566-573.

Yaghjian, A. D. (1975). Upper-bound errors in far-field antenna parameters determined from planar near-field measurements, Part 1: Analysis, *Nat. Bur. Stand., and Tech. Note 667*, 1975.

Yaghjian, A. D. (1986). An Overview of Near-Field Antenna Measurements, IEEE Transactions on Antennas and Propagation, Vol. AP-34, No. 1, January 1986, pp. 30-45.

Advances in Measurement Systems

Edited by Milind Kr Sharma

ISBN 978-953-307-061-2
Hard cover, 592 pages
Publisher InTech
Published online 01, April, 2010
Published in print edition April, 2010

How to reference

In order to correctly reference this scholarly work, feel free to copy and paste the following:

Burgos Sara, Sierra-Castaner Manuel, Martin Fernando, Cano Francisco and Besada Jose Luis (2010). Error Analysis and Simulator in Cylindrical Near-Field Antenna Measurement Systems, Advances in Measurement Systems, Milind Kr Sharma (Ed.), ISBN: 978-953-307-061-2, InTech, Available from: http://www.intechopen.com/books/advances-in-measurement-systems/error-analysis-and-simulator-in-cylindrical-near-field-antenna-measurement-systems

INTECH
open science | open minds

InTech Europe
University Campus STeP Ri
Slavka Krautzeka 83/A
51000 Rijeka, Croatia
Phone: +385 (51) 770 447
Fax: +385 (51) 686 166
www.intechopen.com

InTech China
Unit 405, Office Block, Hotel Equatorial Shanghai
No.65, Yan An Road (West), Shanghai, 200040, China
中国上海市延安西路65号上海国际贵都大饭店办公楼405单元
Phone: +86-21-62489820
Fax: +86-21-62489821

IntechOpen